Negative refraction and sub-wavelength focusing in the visible range using transparent metallo-dielectric stacks

Michael Scalora, Giuseppe D'Aguanno, Nadia Mattiucci, and Mark J. Bloemer

Charles M. Bowden Research Center, AMSRD-AMR-WS-ST, Research, Development, and Engineering Center, Redstone Arsenal, AL 35898-5000
michael.scalora@us.army.mil

Domenico de Ceglia

Dipartimento di Elettrotecnica ed Elettronica, Politecnico di Bari, Via Orabona 4, 70124 Bari, Italy

Marco Centini, AntonioMandatori, and Concita Sibilia

INFM at Dipartimento di Energetica, Universita di Roma 'La Sapienza', Via A. Scarpa 16, 00161 Roma, Italy

Neset Akozbek

Time Domain Corporation, Cummings Research Park 7057 Old Madison Pike Huntsville, Alabama 35806, USA and

Mirko G. Cappeddu

Universita di Roma, Dipartimeno dei Materiali, via Eudossiana 18, I-00184 Rome, Italy

Mark Fowler

Digital Fusion, 5030 Bradford Drive Building 1, Suite 210 Huntsville, AL 35805

Joseph W. Haus

Electro-Optics Program, University of Dayton, Dayton, OH 45469-0245, USA

Abstract: We numerically demonstrate negative refraction of the Poynting vector and sub-wavelength focusing in the visible part of the spectrum using a transparent multilayer, metallo-dielectric photonic band gap structure. Our results reveal that in the wavelength regime of interest evanescent waves are not transmitted by the structure, and that the main underlying physical mechanisms for sub-wavelength focusing are resonance tunneling, field localization, and propagation effects. These structures offer several advantages: tunability and high transmittance (50% or better) across the visible and near IR ranges; large object-image distances, with image planes located beyond the range where the evanescent waves have decayed. From a practical point of view, our findings point to a simpler way to fabricate a material that exhibits negative refraction and maintains high transparency across a broad wavelength range. Transparent metallo-dielectric stacks also provide an opportunity to expand the exploration of wave propagation phenomena in metals, both in the linear and nonlinear regimes.

OCIS codes: (999.9999) Negative index materials; Photonic Band Gap Structures; (310.6860) Thin films; (260.2110) Electromagnetic theory

References and links

1. J. B. Pendry, "Negative refraction makes a perfect lens," Phys. Rev. Lett. **85**, 3966 (2000).

#77357 - $15.00 USD Received 27 November 2006; revised 22 December 2006; accepted 2 January 2007

2. V. G. Veselago, "Electrodynamics of substances with simultaneously negative electrical and magnetic permeabilities," *Sov. Phys. USPEKHI* **10**, 509 (1968).
3. D. O. S. Melville, and R. J. Blaikie, "Super-resolution imaging through a planar silver layer," Opt. Express **13**, 2127 (2005).
4. N. Fang, H. Lee, C. Sun, and C. X. Zhang, "Sub–diffraction-limited optical imaging with a silver superlens," Science **308**, 534 (2005).
5. J. B. Pendry, A. J. Holden, D. J. Robbins, and W. J. Stewart, "Magnetism from conductors and enhanced nonlinear phenomena," IEEE Trans. Microwave Theory Tech. **47**, 2075 (1999).
6. R. A. Shelby, D. A. Smith, and S. Schultz, "Experimental verification of a negative index of refraction," Science **292**, 77- (2001).
7. C. G. Parazzoli, R. B. Greegor, K. Li, B. E. C. Koltenbah, and M. Tanielian, "Experimental verification and simulation of negative index of refraction using Snell's law," Phys. Rev. Lett. **90**, 107401 (2003)
8. V. M. Shalaev, W. Cai, U. K. Chettiar, H-K Yuan, A. K. Sarychev, V. P. Drachev, and A. V. Kildishev, "Negative index of refraction in optical metamaterials," Opt. Lett. **30**, 3356 (2005).
9. G. Dolling, M. Wegener, C. M. Soukoulis, and S. Linden, "Negative index metamaterial at 780nm wavelength," http://arxiv.org/abs/physics/0607135.
10. S. A. Ramakrishna, J. B. Pendry, M. C. K. Wiltshire, and W. J. Stewart, "Imaging the near field," J. Mod. Opt. **50**, 1419 (2003).
11. K. J. Webb and M. Yang "Subwavelength imaging with a multilayer silver film structure," Opt. Lett. **31**, 2130 (2006).
12. B. Wood, J. P. Pendry, and D. P. Tsai, "Directed sub-wavelength imaging using metallo-dielectric system," Phys. Rev. B **74**, 115116 (2006).
13. P. A. Belov and Y. Hao, "Subwavelength imaging at optical frequencies using a transmission device formed by a periodic layered metallo-dielectric structure operating in the canalization regime," Phys. Rev. B **73**, 113 110, (2006).
14. M. Scalora, M. J. Bloemer, A. S. Manka, S. D. Pethel, J. P. Dowling, and C. M. Bowden, "Transparent, metallo-dielectric one dimensional photonic band gap structures," J. Appl. Phys. **83**, 2377 (1998).
15. M. J. Bloemer, and M. Scalora, "Transmissive properties of Ag/MgF_2 Photonic Band Gaps," Appl. Phys. Lett. **72**, 1676-1678 (1998).
16. M. Scalora, M. J. Bloemer, and C. M. Bowden, "Laminated photonic band structures with high conductivity and high transparency: Metals under a new light," Opt. Photon. News **10**, 23 (1999).
17. E. D. Palik, *Handbook of Optical Constants of Solids* (Academic Press, New York, 1985).
18. M. C. Larciprete, C. Sibilia, S. Paoloni, M. Bertolotti, F. Sarto, and M. Scalora, "Accessing the optical limiting properties of Metallo-Dielectric Photonic band gap structures,", J. Appl. Phys. **93**, 5013 (2003).
19. R. S. Bennink, Y. K. Yoon, R. W. Boyd, and J. E. Sipe, "Accessing the optical non-linearity of metals with metallo-dielectric photonic band gap structures" Opt. Lett. **24**, 1416 (1999).
20. N. N. Lepeshkin, A. Schweinsberg, G. Piredda, R. S. Bennink, and R. W. Boyd, "Enhanced nonlinear optical response Metallo-dielectric photonic crystals," Phys. Rev. Lett. **93**, 123902 (2004).
21. M. Scalora, N. Mattiucci, G. D'Aguanno, M. C. Larciprete, and M. J. Bloemer, "Nonlinear pulse propagation in one-dimensional metallo-dielectric multilayer stacks: Ultrawide bandwidth optical limiting," Phys. Rev. E **73**, 016603 (2006).
22. J. D. Jackson, *Classical Electrodynamics*, 2nd edition, (Wiley, New York, 1975).
23. D.R. Smith, D. Schurig, "Electromagnetic wave propagation in media with indefinite permittivity and permeability tensors," Phys. Rev. Lett. **90**, 077405 (2003).
24. D. R. Smith, P. Kolinko, D. Schurig, "Negative refraction in indefinite media," J. Opt. Soc. Am. B **21**, 1032 (2004).
25. R. Wanberg, J. Elser, E. E. Narimanov, and V. A. Podolsky, "Nonmagnetic nanocomposites for optical and infrared negative refractive index media," J. Opt. Soc. Am. B **23**, 498 (2006).
26. A. A. Govyadinov, and V. A. Podolsky, "Material photonic funnels for subdiffraction light compression and propagation," Phys. Rev. B **73**, 155108 (2006).
27. S. Feng, and J. M. Elson, "Diffraction-suppressed high-resolution imaging through metallodielectric nanofilms," Opt. Express **14**, 216 (2006).
28. M. J. Bloemer, G. D'Aguanno, N. Mattiucci, M. Scalora, and N. Akozbek, "Broadband super resolving lens with high transparency for propagating and evanescent waves in the visible range," http://www.arxiv.org/abs/physics/0611162.

1. Introduction

Pendry predicted that a flat slab of an isotropic material having $\varepsilon = \mu = -1$ would make a perfect lens capable of focusing both the far and near field components of a point object, thus achieving super-resolution [1], which refers to the ability to resolve details of an object below

#77357 - $15.00 USD Received 27 November 2006; revised 22 December 2006; accepted 2 January 2007

the Rayleigh limit, set at ~0.6λ. Materials that exhibit simultaneously a negative permittivity and magnetic permeability were first considered by Veselago and termed negative index materials [2]. However, there are no known natural materials that exhibit a negative index of refraction. In order to circumvent this shortcoming, Pendry considered the case where electric and magnetic effects may be decoupled such that for TM-polarization only the requirement that ε=-1 needs to be satisfied. He showed that a thin metal layer acts as a superlens for TM polarized light [1]. The image is formed by negative refraction [2] that occurs inside the metal. The metal transmits evanescent waves and focuses a diverging wave-front to a tight spot inside the medium. The presence of evanescent modes makes it possible for the image to be resolved beyond the limits imposed by ordinary optical materials and by diffraction [1]. If the metal layer is sufficiently thick, and the object is sufficiently close, the light may form a first focus inside the metal layer, and a second focus outside it, where the object is imaged with features that exceed the diffraction limit, i.e. superresolution, as a direct consequence of the preservation of evanescent wave vectors [1]. The effect predicted in reference [1] has been experimentally observed and verified [3, 4].

A shortcoming with the single-layer super-lens is the opacity of metals. The first theoretical predictions and experiments were carried out using silver layers 40-50nm thick, at a frequency just below the plasma frequency, which occurs at ~320nm, where the dielectric constant of silver is negative, and the material is still somewhat transparent. The super-resolution is based on the excitation of surface modes, which evanescently couple the light to the other side of the barrier. In general, transmittance through a single metal layer is rather low, and gets rapidly worse in the visible range and beyond as the wavelength increases. The opacity of metals has thus driven researchers to seek negative refraction and super-lensing by first engineering a negative index material in the microwave regime using metallic rods and loops to induce an electric and magnetic resonance [5-7], and then by seeking a way to scale down the size of magnetic circuits using nano-wires or nano-strips, for example, in order to access the visible region [8, 9]. However, the containment of material and scattering losses in the visible range, along with the successful achievement of size reduction, remain formidable challenges.

In order to reduce the losses incurred in the single metal layer lens, a structures was proposed consisting of alternating layers of metal and dielectric materials having thicknesses much smaller than the incident wavelength [10]. In this arrangement, and in this regime, the structure displays strong anisotropic properties that make it possible for it to behave as a waveguide, with little or no diffraction taking place, in a scheme that helps the formation of a super-resolved image of the object (two apertures) on the exit surface [10]. The problem of extending the use of structures that contain metallic components to the visible range has since been addressed in several publications [11, 12, 13]. The common themes that emerge every time are the inherently large absorption and scattering losses that are not easily overcome.

Historically, the study of the propagation of light in metals has received limited attention because bulk metals are opaque across the entire electromagnetic spectrum. A quasi-transparent region naturally occurs near the plasma frequency, where the real part of the dielectric constant approaches zero, and absorption is minimized. One of the more significant optical properties of a metal is its skin depth, a measure of the distance where the magnitude of the electric field has decreased to approximately 1/3 of its value at the surface. Since metals are very dispersive across the spectrum, the skin depth is a strong function of frequency. For example, the skin depth of silver and other metals such as copper, aluminum and gold, at optical frequencies is approximately 10nm, and at microwave frequencies it is ~1μm. The small skin depth at optical frequencies has motivated the choice of very thin metal layers for applications in the visible range, and so it is not unusual to find designs of metallo-dielectric stacks containing layers that are less than 5nm thick, even in the ultraviolet region [10, 12], in order to access the natural transparency that characterizes noble metals for such thicknesses. Unfortunately, multilayer stacks composed of very thin layers are difficult to fabricate in

#77357 - $15.00 USD Received 27 November 2006; revised 22 December 2006; accepted 2 January 2007

practice.

2. Metallo-Dielectric Photonic Band Gap Structures: Resonance Tunneling

In this paper, we consider a configuration based on metallo-dielectric photonic band gap structures. It has already been shown, both theoretically and experimentally, that it is possible to significantly curb absorption and scattering losses in the visible range using metallo-dielectric photonic band gap (MD-PBG) structures [14-16]. Although the concept of transparent MD-PBGs has already been discussed in our previous work, here we review some of the important features that are relevant to the current studies. Transparent, MD-PBGs are based on the principle of photonic band gap materials consisting of alternating two different materials having different indices of refraction. A typical structure may contain several metallic layers, each tens of nanometers or many skin depths thick, so that individual metal layers may be relatively opaque. Resonant tunneling occurs for those wavelengths that are resonant with the metal cavities that are stacked together to form the photonic band gap structure. Metal layer separation is typically chosen to be ~λ/4-λ/2, where λ is the tunneling wavelength in the medium. Since the index of refraction for most metals is of order unity or less in the visible range, interference effects tend to change the resonance tunneling condition away from the characteristic λ/2 thickness, and to allow mostly unimpeded propagation of light with minimal scattering and absorption losses [14-16]. Modifications of the resonant

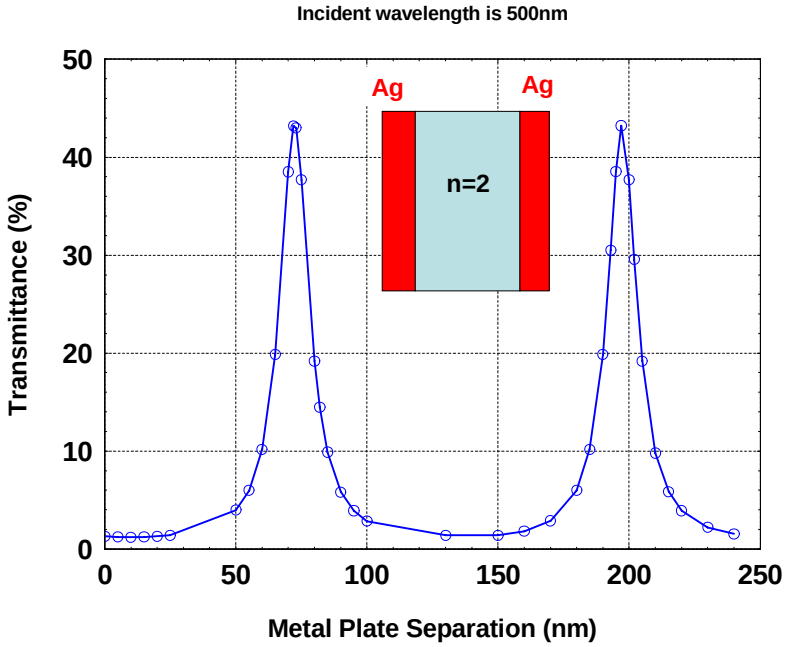

Fig. 1. Transmittance vs. separation distance between two metal layers 32nm thick, for a dielectric spacer medium having n=2 (inset), and incident wavelength of 500nm. The resonance tunneling condition occurs for dielectric layer thickness of 72nm, or 0.29λ, where λ is the wavelength in the material.

tunneling condition can be observed in the simple case of a metallic Fabry-Perot cavity. We depict this situation in Fig. 1, where we plot the transmission as a function of the separation between two metal layers approximately 32nm thick, and use actual material data for 500nm incident light [17]. Although the dielectric spacer is assumed to have n=2, similar considerations hold for arbitrary index. In the figure, a transmission resonance can be observed for plate separation of ~72nm, and then again for ~197nm. These conditions are

#77357 - $15.00 USD Received 27 November 2006; revised 22 December 2006; accepted 2 January 2007

actually quite far from the more familiar λ/2 condition (or multiples of it), which is 125nm for n=2. This relatively large shift is due to the finite thickness of the metal layers, and to the fact that we are not using a perfect conductor. As a result, resonance tunneling is pushed closer to a thickness of ~λ/4, and to non-integer multiples of it. In general, the resonance tunneling condition depends on tuning, metal and dielectric layer thickness, and index of refraction.

Even though these shifts are easy to understand, the most surprising aspect of resonance tunneling in MD-PBGs is that the addition of more, thick metal layers does not reduce the maximum transmission [14-16], as we will see below. A typical transparent metal stack may contain hundreds of nanometers of metal, and it can have transparencies well above 50%, within pre-selected, broad wavelength ranges, across the entire visible region and well beyond. The location of the transparency window depends on the thickness of the intervening dielectric material, and can be engineered by using a combination of appropriate metals, and/or dielectric materials, from the visible well into the mid-infrared range. For instance, one may use almost any dielectric or semiconductor material, in combination with aluminum (for work in the ultraviolet range), silver (best used in the visible part of the spectrum), gold, and copper (both better suited for near-infrared applications). As an example, an 11-layer, Ag/MgF_2 stack containing 150nm of silver was fabricated [15, 16] using thermal evaporation techniques, that featured a peak transmittance of about 52% at 532nm, with a full width at half maximum well in excess of 100nm. Metal layer thicknesses ranged from a low of 20 to a high of 40nm, and so it is possible to further increase transmittance by thinning out Ag layers, and by choosing a material with a relatively high index of refraction, such as ZnO [18] or TiO_2. We note that nonlinear effects have also been studied in Cu/SiO_2 stacks similar to those that we describe here, both theoretically [19] and experimentally [20]. In reference [20], for example, the localization of the light inside the Cu layers was confirmed by directly measuring nonlinear phase and transmittance changes as a function of incident intensity.

Given these structures' ability to be transparent in the visible range and beyond, even when hundreds of nanometers of metal are present, we are thus naturally led to ask the following question: could transparent, MD-PBGs be useful for the purposes of achieving negative refraction and/or sub-wavelength imaging in the visible range? Since metal is required for the anomalous refraction process described in reference [1] to occur, it would seem that a combination of transparency and metals should yield an affirmative answer to our query. Therefore, we set out to study propagation effects in these structures, in a regime where each metal layer may be several tens of nanometers thick and be relatively opaque, and typical dielectric layer width is between one quarter- and a half-wavelength thick. This combination sets the stage for the resonance tunneling phenomenon to occur, which in our case regulates every aspect of the passage of the light through the stack. The propagation effects that we discuss thus relate to the ability to localize light *inside* individually thick metal layers to increase local energy and momentum values [20, 21]. As a result, surface waves are *not* necessarily excited inside the stack, and we report negative refraction and sub-wavelength focusing in transparent metal stacks due to propagating rather than evanescent modes, a combination that makes these findings unique. As we will show below, these structures can have high transparency for both the propagating and evanescent waves. However, in this paper we concentrate on the propagating modes which are important if the object or image plane is far from the lens. While the relative absence of evanescent modes at the external focus may not make this device the most efficient in terms of resolving power, the stack amounts to a lens that extends the regimes accessible using any single metal layer [1], or by using densely-packed, thin, non-resonant metallo-dielectric layers [10]. In addition to providing new opportunities to study wave propagation phenomena inside metals, transparent MD-PBGs may also be attractive because they have already been fabricated and their operation tested against model calculations. Resonance tunneling has been experimentally verified in the visible range, in both linear and nonlinear regimes, and it is discussed in details in references [14-21]. The propagation model that we use is described in details elsewhere

#77357 - $15.00 USD Received 27 November 2006; revised 22 December 2006; accepted 2 January 2007

[21]. Here we simply state that we use a pulse propagation model that integrates the vector Maxwell's equations in the time domain with two spatial coordinates and time, that includes proper treatment of material dispersion and absorption. The integrations are carried out using a time-domain, fast Fourier transform based algorithm [21], and the results show good convergence for a longitudinal spatial discretization of ~3.57nm, a sampling of the transverse coordinate of ~12.5nm, and a time step of ~1.19×10^{-17} sec.

3. Propagation effects inside the Transparent Metal Stacks: Negative Refraction

To illustrate the negative refraction process through a transparent metal lens, we examine the propagation of short, sub-picosecond pulses through a Ag/dielectric stack. We define a transparent metal as a series of coupled Fabry-Perot cavities with anti-reflection (AR) coatings at the entrance and exit faces of the stack. The AR coatings are 1/2 the thickness of the internal dielectric layers and of the same material. The transparent metal under discussion is a 5.5 period Ag(32nm)/X(21nm) stack, where X represents a generic material having refractive index n=4, and AR coatings of X(11 nm) at the entrance and exit of the stack. The transparent metal thus contains 192nm of silver, and it is approximately 318nm thick. This particular choice of entry and exit layer thicknesses is crucial because it single-handedly increases the transmittance many times across the transparency range, and can also significantly change the field localization characteristics inside the stack compared to those of a periodic structure without the AR coating [21]. As an example, in Fig. 2 we depict the plane-wave transmittance as a function of wavelength for normally incident light, for the transparent metal and a structure that has six periods of Ag(32nm)/X(21m). The two structures are shown in the inset, and they are almost identical were it not for the disposition of the first and last layers. A cursory look at the curves suggests that the degree of transparency can be drastically different, and proper design can thus fulfill the demand for adequate transparency anywhere in the visible range [16, 21].

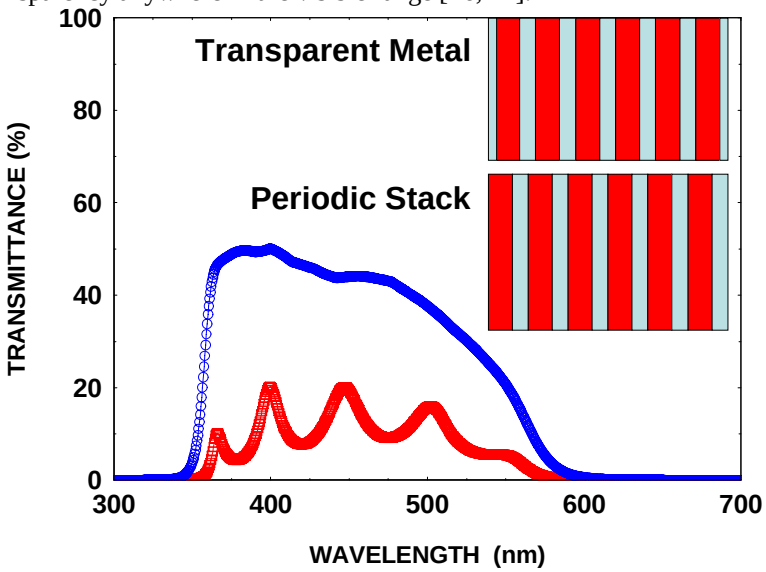

Fig. 2. Plane-wave transmittance vs. wavelength at normal incidence from a symmetric, 13-layer stack composed of Ag(32nm)/X(21nm), inclusive of entry and exit X layers 11nm thick (transparent metal), and from a periodic stack composed of 6 periods of Ag(32nm)/X(21nm). Halving the thickness of first and last layers increases transmittance significantly across the transparency range, and affects field localization properties (Fig. 8 below).

Increasing dielectric layer thickness (even by factors of two) generally redshifts the location of the transparency window without impacting the transmittance to a significant degree. The basic characteristics that these structures share is that light can actually dwell inside the metal

#77357 - $15.00 USD Received 27 November 2006; revised 22 December 2006; accepted 2 January 2007

layers without being completely absorbed, a fact that is reflected in experimental observations [15, 16, 18, 20]. The metal layers thus feature the simultaneous localization of both electric and magnetic fields. When combined with the transparency of the stack, the stack's ability to store energy and momentum with minimal scattering or absorption losses translates into a

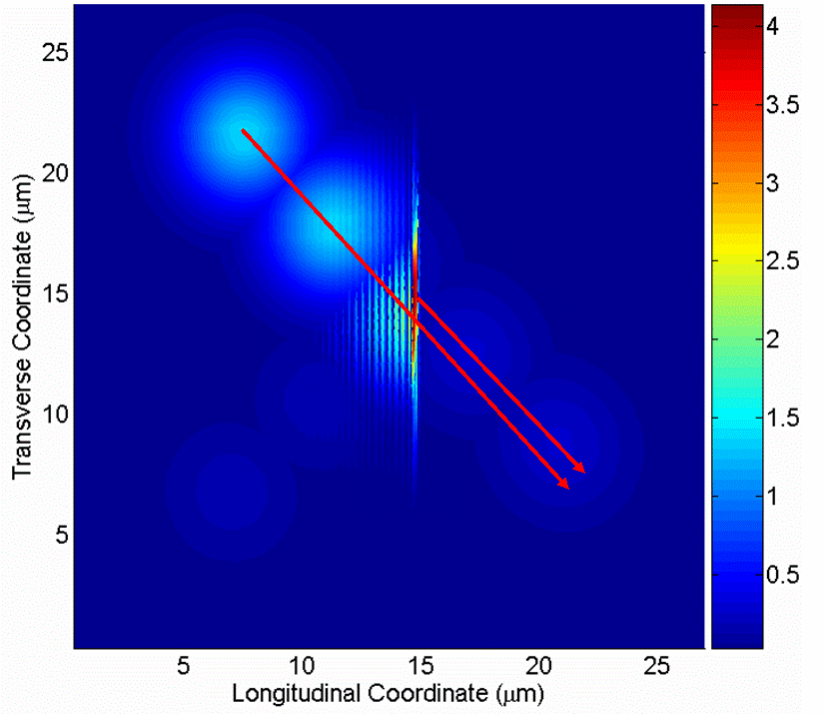

Fig. 3. A Gaussian, TM-polarized wave packet is incident at 45° on the transparent metal stack described in Fig. 2. The figure shows several snapshots of the magnetic field intensity. The centroid of the pulse that exits to the right of the stack is shifted upward by approximately 266nm. Plane-wave reflectance is ~5% at 400nm.

relatively efficient negative refraction process, with negative angles that can easily approach 45º, as we will see below.

As an example, we tune the carrier wavelength of an incident pulse at 400nm, and launch it with an incident angle of 45º. At this wavelength the dielectric constant of Ag is $\varepsilon = -3.77 + i0.67$ [17]; at this angle the transmittance and reflectance of the stack are ~30% and ~5% respectively. We note that we use actual material data already tested and verified specifically for transparent metal stacks [14-21]. For simplicity, but only for the moment, we assume that material X is dispersion-less and absorption-less, that our incident pulse is Gaussian, $H(\xi, \tilde{y}, \tau = 0) = H_0 e^{-(\xi^2 - \xi_0^2)/w_\xi^2} e^{-(\tilde{y}^2 - \tilde{y}_0^2)/w_{\tilde{y}}^2}$, and that $w_\xi = w_{\tilde{y}}$, so that the spatial width translates to a ~30fs duration (1/e width). At the carrier frequency of 400nm the pulse is ~20 optical cycles in duration; this means that the curvature of the wave front changes imperceptibly and there are no extra complications due to diffraction over the entire propagation distance. Figure 3 contains several snapshots that chronicle the dynamics of the pulse as it traverses the stack. The centroid of the transmitted wave packet appears to be shifted upward, a detour that is best perceived for short, well-localized wave packets, but that clearly holds for any pulse of larger but finite spatial extension and longer temporal duration. This shift can only be understood in terms of additional upward momentum supplied to the pulse by the structure, and is associated with the negative refraction of the Poynting vector.

The lensing effect described in reference [1] is based on a change in direction of the

#77357 - $15.00 USD Received 27 November 2006; revised 22 December 2006; accepted 2 January 2007

longitudinal component of the electric field, which points along the direction of propagation, and that brings about a change in direction of the Poynting vector. In other words, the Poynting vector of a TM-polarized beam, obliquely incident on a metal surface or layer, refracts with a negative angle inside the metal. We depict this situation in Fig. 4. It is the continuity of the longitudinal component of the electric displacement field, **D**=ε**E,** at the

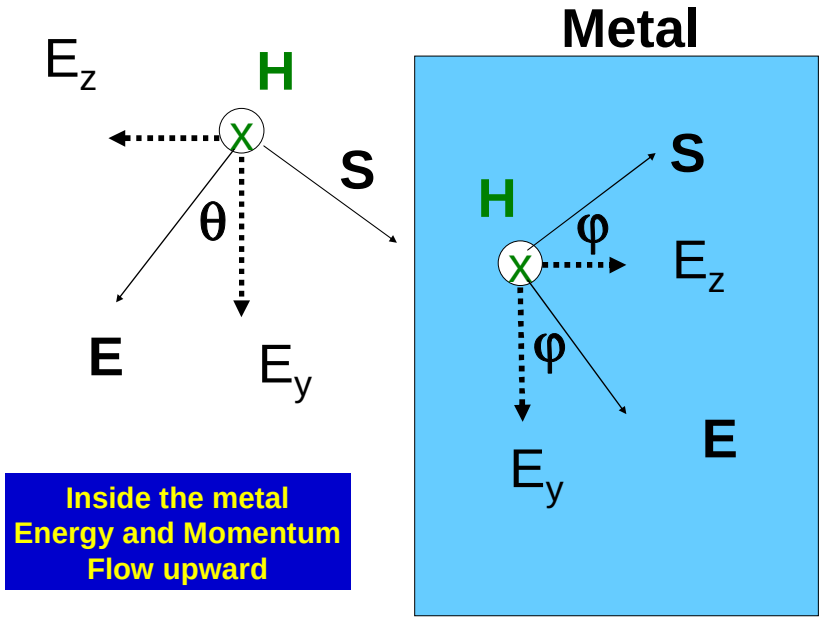

Fig. 4. A TM-polarized beam or pulse is incident from vacuum (or other medium with positive permittivity) on a metal layer, at frequencies below the plasma frequency where the real part of its dielectric constant is negative. The x inside the circle indicates that the **H** field points inside the page. Then, preservation of the continuity of the longitudinal component of the displacement field, $D_z^{out} = D_z^{in}$, requires that $\varepsilon_{out} E_z^{out} = \varepsilon_{in} E_z^{in}$. As a result, a sign change of the field E_z occurs when the dielectric constants have opposite signs.

boundary between two adjacent media that have opposite dielectric constants, that forces the change in the direction of propagation of the Poynting vector. For a pulse of finite spatial extension, the negative refraction process is best described by calculating the electromagnetic momentum inside the stack as a function of time, as the pulse sweeps across the structure. The results are summarized in Fig. 5. The total electromagnetic momentum may be defined as usual [22]: $\mathbf{P}(t) = \int_{z=-\infty}^{z=\infty} \int_{y=-\infty}^{y=\infty} \frac{\mathbf{S}(y,z,t)}{c^2}\, dy\, dz = \int_{z=-\infty}^{z=\infty} \int_{y=-\infty}^{y=\infty} \frac{\mathbf{E}\, x\, \mathbf{H}}{4\pi c} dy\, dz$ where y and z are the transverse and longitudinal coordinates, respectively. Although the quantities we calculate are generally instantaneous, one may proceed by either performing a time average as the pulse dwells inside the stack, or by simply taking the most dominant values, which occur when the peak of the pulse arrives at the structure, in order to mimic near plane-wave conditions. We find that the total average momentum vector, when the peak of the pulse reaches the stack, refracts upwardly as shown, forming an angle of~-40º with respect to the normal. Given a structure length of ~318nm, the calculated upward shift is δ~266nm. Furthermore, calculations similar to those exemplified in Fig. 5 were carried out for incident angles of 15º and 30º. The resulting momentum refraction angles are ~-14º and ~-27º, respectively. Note that this is not a perfect lens condition for negative refraction. In the perfect lens, the incident and refracted angles have the same magnitude because the space

#77357 - $15.00 USD Received 27 November 2006; revised 22 December 2006; accepted 2 January 2007

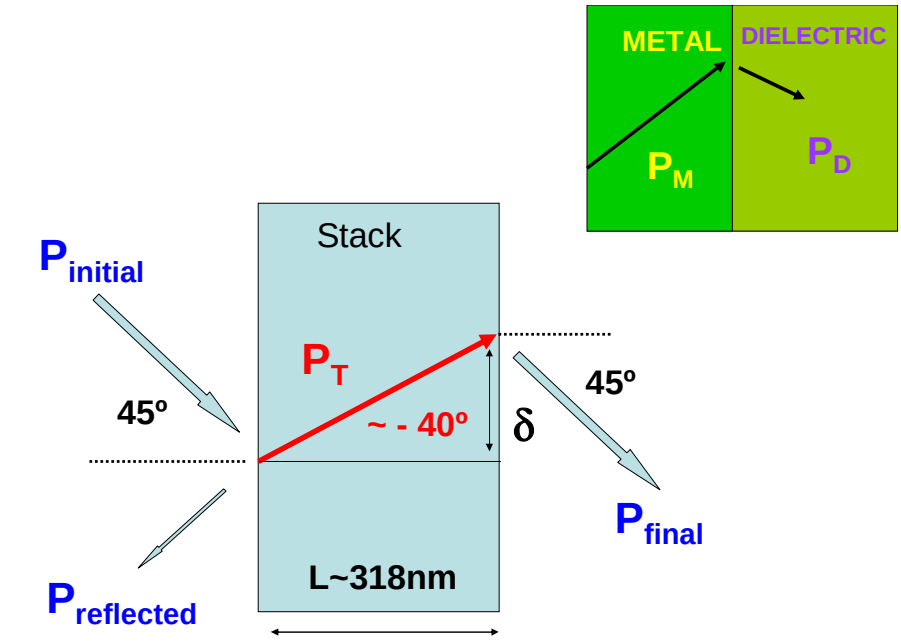

Fig. 5. Schematic representation of the refraction that occurs inside the stack. $\mathbf{P}_T$ is the total, averaged momentum inside the stack. Upper right: the local momenta inside two adjacent metal and dielectric layers are shown. The local momentum density, i.e. the Poynting vector, generally differs from the total momentum within a given layer. The refraction process should be viewed from a global perspective, by collecting information across the entire layer.

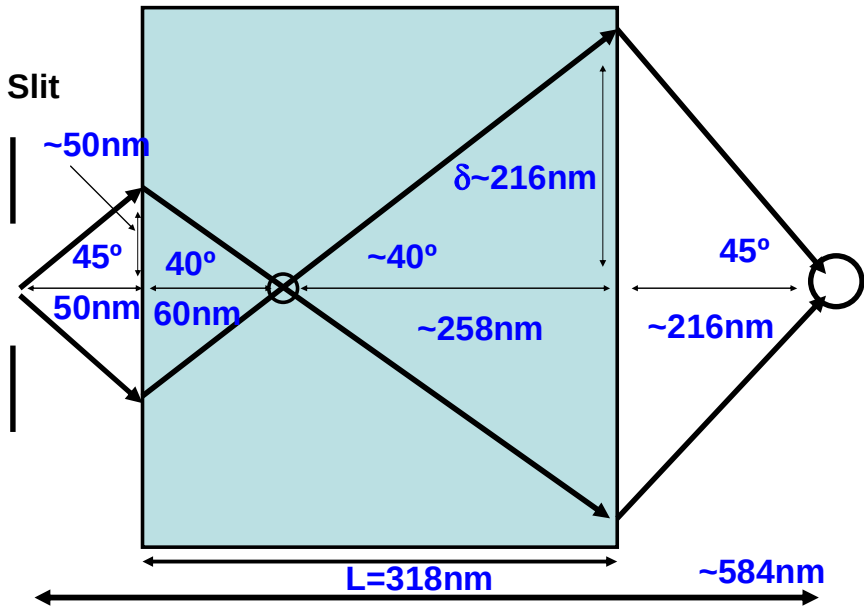

Fig. 6. Schematic representation of twin momentum vectors that lead to the formation of internal and external foci, based on the results depicted in Fig. 5. In this picture the location of both foci are approximate, as the averaging process neglects effects of field curvature. Both internal and external focal points generally depend on the slit-stack distance.

#77357 - $15.00 USD Received 27 November 2006; revised 22 December 2006; accepted 2 January 2007

preceding the lens has an index of refraction equal to, but opposite, that of the lens. Although the lens is not "perfect", it is a realistic lens, and as we will see below, it retains sub-wavelength focusing properties.

The approximate dynamics that ensues for typical twin momentum vectors emanating at ~45º from a narrow slit is shown in Fig. 6. The picture that emerges suggests that two foci should form, one inside the stack, and a second approximately 216nm away from the stack. We emphasize that both Figs. 5 and 6 are only schematic renditions of what actually occurs, because ultimately the momentum density (i.e. the Poynting vector) is a local, instantaneous quantity subject to variations dictated by local field curvature and localization. A similar reconstruction done for the two sets of twin momentum vectors incident at 15º and 30º, also emanating from an aperture ~50nm away from the stack, yields focal positions of ~246nm and ~230nm, respectively. The geometry suggests that the estimated focal positions also vary depending on the aperture-multilayer distance. These propagation exercises thus reveal that a diffracting wave containing a span of transverse k-vectors, emanating from a small aperture and traversing the transparent metal stack, will tend to form an extended focus having a rough diameter of ~20-30nm.

Now that we have established that negative refraction occurs in the visible range, we wish to test the performance of this particular structure across the transparency window. The situation is depicted in Fig. 7, where we plot the negative refraction angle as a function of

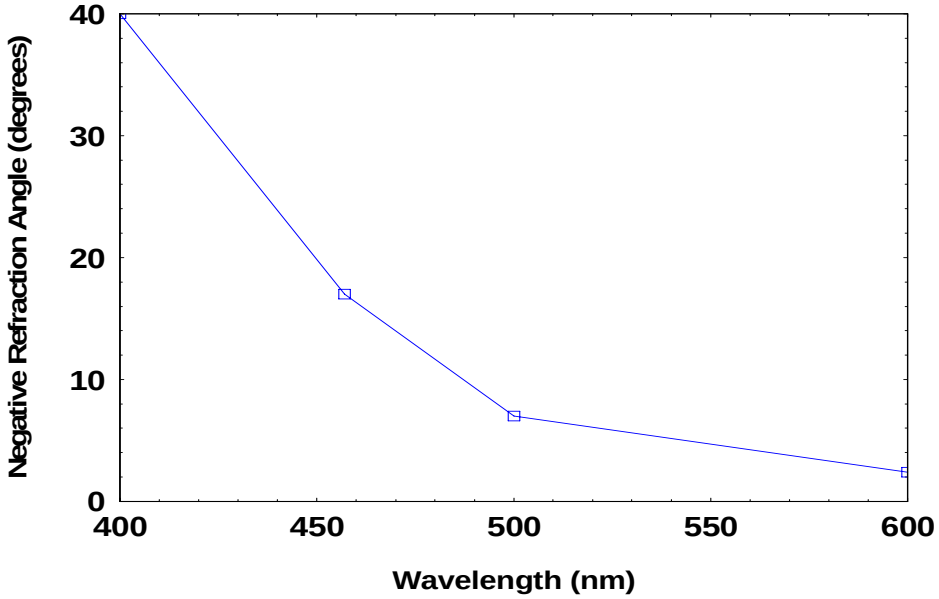

Fig. 7. Negative refraction angle as a function of incident wavelength. The incident angle is fixed at 45º. The angle decreases as the carrier wavelength is increased. This is due in large part to the metal dispersion, which causes a drop in the magnetic field intensity inside the metal layers only, resulting in a reduction of anomalous momentum.

incident wavelength, for an incident angle fixed at 45º. Although the basic cause and effect for the pattern that emerges is quickly identified, namely that the magnitude of the dielectric constant of silver eventually overtakes that of the dielectric material (ε=16) at longer wavelengths, more is at play here than just the ratio of dielectric constants. At 400nm, the magnitude of the ratio between the real parts of the dielectric constant is 16/3.77. At 500nm the ratio drops to 16/8.57, and by the time we reach 600nm the ratio is ~16/14. So a measure of transmittance, which may be higher at 500nm relative to 400nm, for example, is not always a good indicator of how the stack may perform. This effect is due to the large degree of material dispersion that impacts the metal in transitioning toward longer wavelengths,

#77357 - $15.00 USD Received 27 November 2006; revised 22 December 2006; accepted 2 January 2007

resulting in large variations in the localization properties of the magnetic field. More specifically, Fig. 8 depicts the electric and magnetic field intensities for normal incidence at 400nm. At 500nm the electric field intensity changes little across the stack, but the magnetic field intensity drops by an average factor of three only inside the metal layers. This dynamical behavior impacts the Poynting vector, and causes a simultaneous drop in anomalous momentum and negative refraction angle. We remark that the momentum refraction process is generally always anomalous (upper, right quadrant in Fig. 5 in each metal layer, just as it occurs for the isolated metal layer in Ref. [1], and normal (lower, right quadrant in Fig. 5) in each dielectric layer. However, given the high degree of

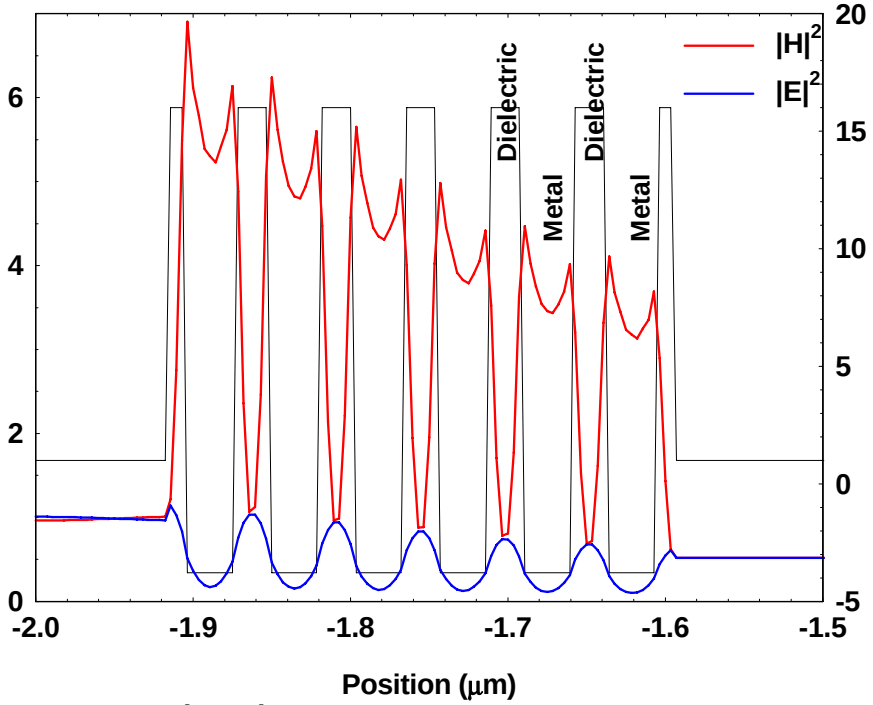

Fig. 8. On-axis $|E|^2$ and $|H|^2$ vs. position inside the chirped stack described in Fig. 2, for a field incident from the left. The real part of the dielectric constant alternates between the values of 16 and -3.77 (thin, black curve; right axis). The fields are unusually intense inside each metal layer, leading to large energy and momentum values inside each metal layer. At 500nm, for silver Re(ε)= -8.57. The shape and amplitude of the electric field intensity change little across the stack. While the shape of $|H|^2$ remains almost identical, it decreases by an average factor of 3 only inside the metal layers, causing a drop in stored anomalous momentum, and a consequent reduction of the negative refraction angle.

transparency that may be achieved, our multilayer stack effectively extends the operational range of negative refraction well into the visible range and beyond. This aspect of the dynamics is shown in the inset of Fig. 5, where the arrows depict the momentum vectors in each type of layer; the direction of each strongly depends on field localization properties, which in turn may be controlled by the relative amounts of metal and dielectric material. The high index of refraction in the dielectric layer leads to smaller refraction angles inside that layer. At the same time the electric and magnetic fields become localized inside the metal layers in almost equal measure compared to the dielectric layers [14-21]. We note, however, that a high index of refraction is not strictly required for negative refraction: lower indices lead to smaller negative refraction angles. To summarize this section, the transparent metal that we have considered contains individually thick metal and dielectric layers. In the case of negative refraction, the coupled-cavity environment acts as a catalyst for the simultaneous

#77357 - $15.00 USD Received 27 November 2006; revised 22 December 2006; accepted 2 January 2007

localization of magnetic and electric fields inside relatively thick metal layers, to yield an unusually large momentum and energy concentration that may be exploited in various ways, for instance, to access the large $\chi^{(3)}$ of copper [19-21].

4. Focusing properties: Sub-wavelength resolution

Up to this point we have only addressed the issue of the existence of negative refraction. However, we also wish to know whether or not it is possible to resolve an object at or near the Rayleigh limit in the negative refraction regime. Although the issue of near-field focusing has been addressed in different types of media, especially having anisotropic permittivity [12, 23-26], we are deliberately focusing here on propagation effects inside resonant, metallo-dielectric photonic band gap structures to illustrate the new opportunities that they offer. One previous study had discussed the ability of these types of structures to slow down the diffraction process in a different regime [27].

In a related paper it was shown that transparent metals have high, broadband transmittance for evanescent waves [28]. In the present paper we investigate a regime where propagating modes dominate, and so we operate at wavelengths where the transmittance of the evanescent waves is low [28]. To demonstrate the focusing

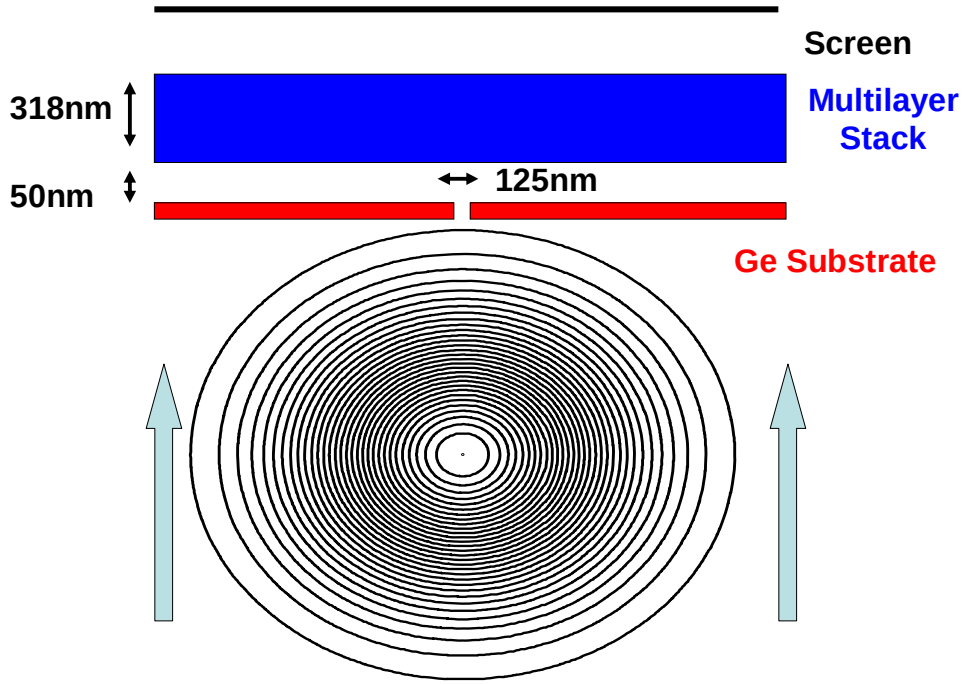

Fig. 9. A quasi-monochromatic Gaussian wave packet is incident from the bottom on a 140nm-thick germanium substrate with an aperture ~125nm wide. The transparent metal stack is described in the caption of Fig. 2, and is located ~50nm away from the slit. The distance to the collection point (screen) may vary.

capabilities of our stack, we begin by once again considering a pulse tuned at 400nm, but this time it is incident on a 140nm-thick, opaque germanium substrate with an aperture ~125nm wide. Without the aperture, the substrate displays a calculated reflectance of ~47%, and a transmittance of ~0.001% [17]. The situation is quite realistic because it takes into account edge effects and the finite depth of the aperture, and it is schematized in Fig. 9. In this example, the slit is located ~50nm away from the stack. Figure 10 captures a snapshot of the

#77357 - $15.00 USD Received 27 November 2006; revised 22 December 2006; accepted 2 January 2007

magnetic field intensity as the peak of the pulse just reaches the stack. Part of the wave packet forms a slightly extended focus just passed the stack, at an approximate distance of 200nm, consistent with the average momentum picture (the location of the internal focal point is also estimated well in Fig. 5. In Fig. 11 we plot the respective, relative field intensities (longitudinal and transverse electric fields) at an approximate distance of ~200nm from the stack, as a function of the transverse coordinate. The slit casts a bright, discernable spot, with a full width at half maximum ~200nm wide, with an incident wavelength about three times larger than slit size. In comparison, the transverse profile of a field diffracting in free space from a similar slit is approximately five times broader at the same location. This minimum width is determined by the spectral characteristics of the transmission function of the stack at hand, and by the degree of excitation of evanescent modes, which as we will see below is minimal in this case. Nevertheless, the focusing capabilities of the stack are already evident in Figs. 10-11, and they are substantial, considering the amount of metal we are using and the distances involved: the object-image distance is ~ 600nm.

In Fig. 12 we depict the magnetic field intensity's interference pattern that results when the pulse is incident on two adjacent apertures 125nm wide, separated by an opaque region ~200nm thick. With reference to Fig. 10 and Fig. 12, it is clear that there are qualitative

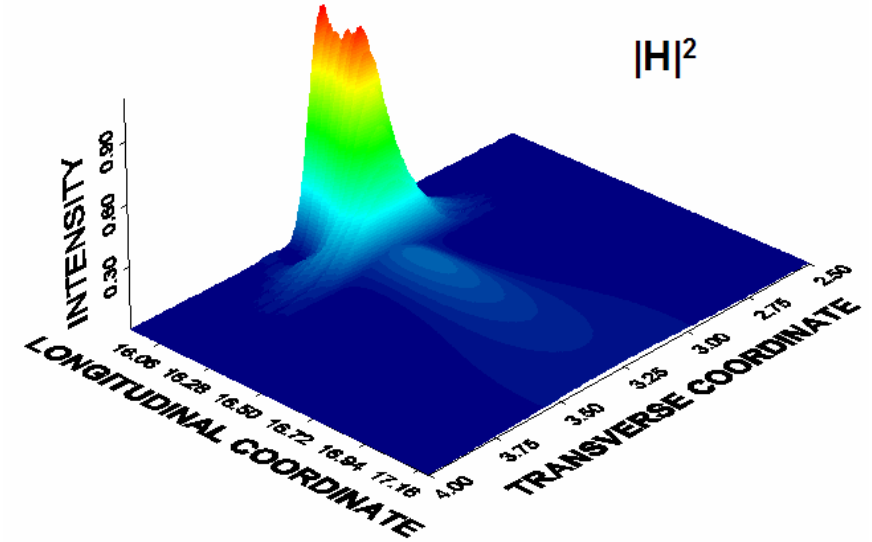

Fig. 10. Bird's eye-view of a snapshot of the magnetic field intensity inside and passed the stack. A focal point is clearly visible outside the stack.

aspects of the interaction that persist in the formation of both internal and external foci, although the interference pattern inside the stack is more complex for the double slit. For example, in Fig. 12 a third bright spot develops further downrange, and comes as a result of interference of the main external foci: side by side the foci become secondary sources that interfere constructively along the longitudinal axis, giving rise to a classic Poisson spot phenomenon. In order to gauge the relative importance of evanescent modes, in Fig. 13 we plot the quantity $S_z(k_y/k_0,z)$, which is the Fourier transform along the transverse coordinate of the longitudinal Poynting vector $S_z(y,z)$. This quantity reveals the spectral content of the fields inside and just outside the stack, and confirms that evanescent k-vectors are largely absent inside the stack. Although the conditions that we have studied are not optimized for maximum visibility, we already see evidence of sub-wavelength resolution without the excitation of evanescent modes or surface waves. The performance of this particular device

#77357 - $15.00 USD Received 27 November 2006; revised 22 December 2006; accepted 2 January 2007

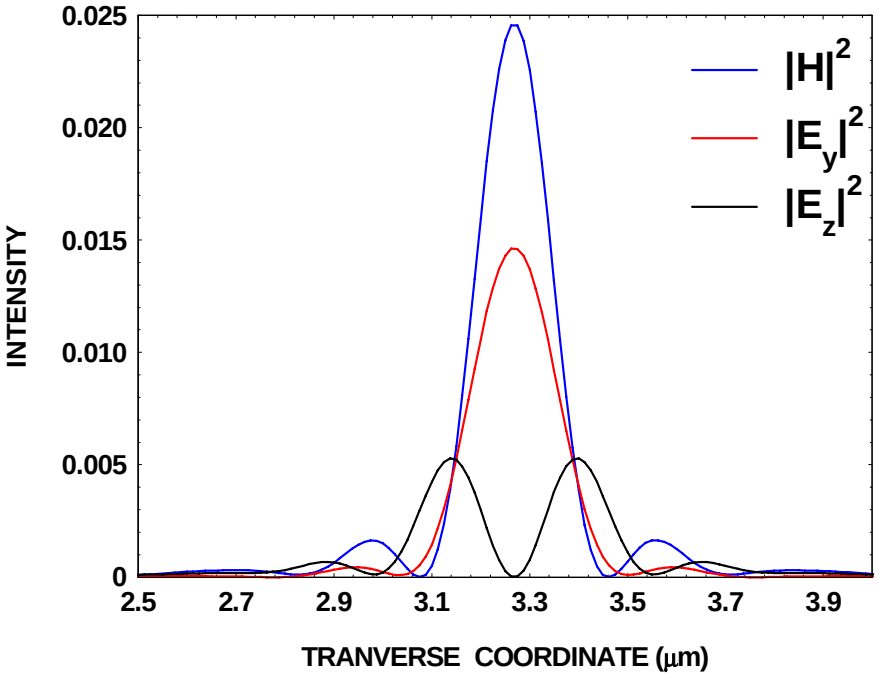

Fig. 11. Image produced by the slit on the image plane indicated on Fig. 9. The full width at half maximum of the H-field that propagates through the stack is ~200nm and it is roughly five times narrower compared to the same field propagating in free space.

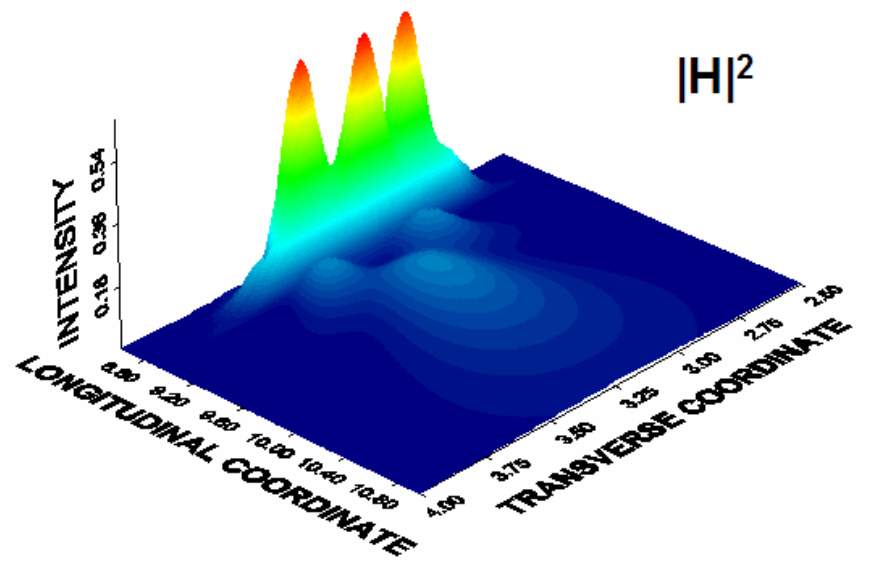

Fig. 12. Bird's eye-view of a snapshot of the magnetic field intensity inside and passed the transparent metal stack. The image is produced by two 125nm apertures located on the Ge substrate, having a center-to-center distance of ~325nm. The slits are resolved with a visibility of approximately 40%, yielding diffraction-limited, sub-wavelength resolution. A third bright spot, Poisson' spot, appears down-range, as a result of constructive interference between the primary spots, which in turn become secondary sources in the Poisson' spot formation process.

should be assessed considering that: (i) we are operating in the visible range; (ii) the object is

#77357 - $15.00 USD Received 27 November 2006; revised 22 December 2006; accepted 2 January 2007

located ~50nm away from the stack; (iii) the object-image distance is more than one wavelength. We note, however, that it is possible to find regimes and/or alternative geometry that will better lend themselves to the realization of a super-resolving, transparent metal lens [28].

5. Closing remarks

We have identified several candidates that are suitable in the visible range, for example TiO_2, Si, GaP, and GaAs. The indices of refraction of Si and GaAs are above 4, while that of GaP is between 3 and 4. Although bulk Si and GaAs are opaque in the visible range, a number of relatively thin but resonant layers may be combined with varying thicknesses of Ag to yield a transparency range, as a simple, standard, matrix-transfer calculation reveals. For instance, we find that a chirped, 13-layer stack composed of Ag(32nm)/Si(22nm), with first and last layers 11nm thick, yields a transmittance window centered around 500nm (where the real part of the dielectric constant of Si is ~18), with maximum transmittance of ~20%. At this wavelength, our model yields a negative refraction angle of ~ -10º. Even though GaP has a lower index of refraction than Si, one may obtain substantially similar results with a stack that contains almost 260nm of Ag. Finally, at 632nm we find that the transmittance from a chirped stack composed of Cu(32nm)/Si(43nm) is still approximately 30%, and yields a negative refraction angle of ~ -3º. So, it is possible to find common materials and to design transparent metal stacks, and still have negative refraction and sub-wavelength resolution occur in the visible range.

In conclusion, we have presented theoretical evidence that negative refraction and sub-wavelength focusing, above the Rayleigh limit, can occur throughout the visible range in transparent, metallo-dielectric, photonic band gap structures, in a regime dominated by propagating modes. These structures may contain hundreds of

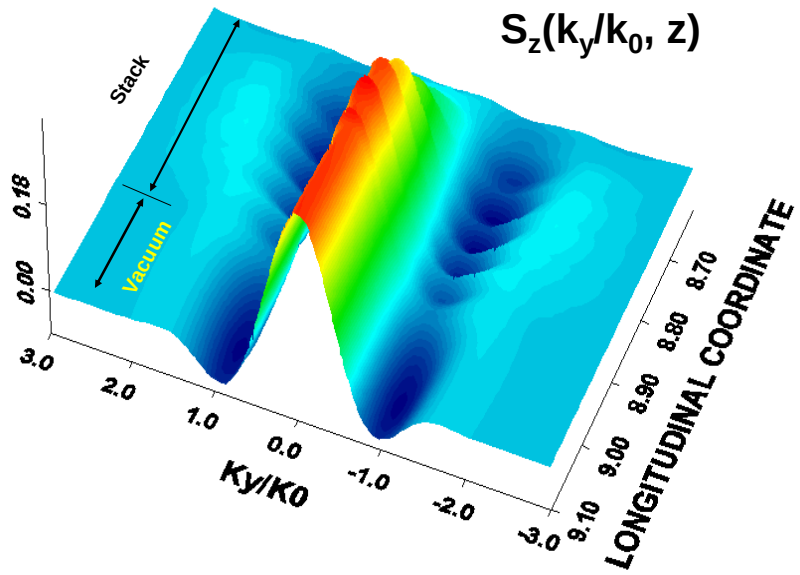

Fig. 13. $S_z(k_y/k_0,z)$ is the Fourier transform of the longitudinal Poynting vector $S_z(y,z)$. The contiguous arrows to the left indicate the beginning and the end of the stack, and where vacuum begins. This spectral snapshot reveals the longitudinal dynamics of each transverse k-vector. It is evident that in this example evanescent wave vectors (ky/k0>1) are hardly excited, an indication that in this regime surface waves are not supported.

nanometers of metal, and yet they can be transparent to visible light and beyond. Our simulations show that incident TM-polarized waves undergo negative refraction, and that

#77357 - $15.00 USD Received 27 November 2006; revised 22 December 2006; accepted 2 January 2007

further optimizations and improvements are possible [28]. These results open a new point of view regarding the propagation of light in metals, and may help pave the way to the achievement of practical devices and applications based on negative refraction, with realistic numerical apertures. Since transparent metal structures have already been fabricated in the visible part of the spectrum using a number of different dielectric materials, the experimental realization of negative refraction in such structures presents no new discernable technical challenges. Taken together with the tunable aspects of the process, which we have touched upon, the search for suitable, high-index materials may yield candidates that could also make it possible to further increase the object-lens distance, and to push the process well into the infrared region of the spectrum, with possible, significant applications to IR imaging.

Acknowledgments

G. D. and N. M. thank the National Research Council for financial support. D. de C. and M. G. C. thank the US Army European Research Office-London for partial financial support.

#77357 - $15.00 USD Received 27 November 2006; revised 22 December 2006; accepted 2 January 2007